Metallographic and Numerical Methods Investigations about Failure of a Kaplan Turbine Runner Blade

DOINA FRUNZAVERDE
Center for Research in Hydraulics, Automation and Thermal Processes – CCHAPT
"Eftimie Murgu" University of Resita
P-ta Traian Vuia 1-4, RO-320085 Resita
ROMANIA
d.frunzaverde@uem.ro; http://www.cchapt.ro/
VIOREL CÂMPIAN
Center for Research in Hydraulics, Automation and Thermal Processes – CCHAPT
"Eftimie Murgu" University of Resita
P-ta Traian Vuia 1-4, RO-320085 Resita
ROMANIA
v.campian@uem.ro; http://www.cchapt.ro/
DORIAN NEDELCU
Center for Research in Hydraulics, Automation and Thermal Processes – CCHAPT
"Eftimie Murgu" University of Resita
P-ta Traian Vuia 1-4, RO-320085 Resita
ROMANIA
d.nedelcu@uem.ro; http://www.cchapt.ro/
GILBERT-RAINER GILLICH
Center of Advanced Research, Design and Technology – CARDT
"Eftimie Murgu" University of Resita
P-ta Traian Vuia 1-4, RO-320085 Resita
ROMANIA
gr.gillich@uem.ro; http://www.cardt.ro/
GABRIELA MĂRGINEAN
Laboratory for Material Science and Material Testing
University of Applied Sciences Gelsenkirchen
Neidenburger Str. 10, D-45877 Gelsenkirchen
gabriela.marginean@fh-gelsenkirchen.de; http://www.fh-gelsenkirchen.de/

Abstract: The paper presents the results of the failure analysis of a Kaplan turbine runner blade from a hydropower station in Romania. In order to determine the causes that led to the cracks, the authors first carried out metallographic investigations on a sample obtained from the cracked blade. The metallographic investigations included macroscopic and microscopic examinations (light microscopy and scanning electron microscopy) and X-ray diffraction analyzes (XRD). They led to the conclusion that the cracking of the blade was caused by fatigue, initiated by the numerous non metallic inclusions, which were discovered in the vicinity of the blade surface. The results obtained were confirmed by calculations on the resistance and service life estimations of the blade. The calculations carried out included the following steps: construction of the solid 3D-model of the blade, determination of the blade loads from hydrodynamic conditions, linear static analysis of the blade and service life estimations, calculated for maximal stress values of the concentrators. They led to the conclusion that the cracking of the blade started and developed from the stress concentrator placed between blade and blade flange on leading edge direction. In order to decrease the maximal stress value, the authors concluded that the hydrodynamic loads on the blade must be obligatory reduced. Therefore, as the operating conditions (discharge, head, speed, power) are not changeable, the stress reduction could be realized only by increasing the number of the runner blades.

Key-Words: Hydropower station, Kaplan turbine, fatigue cracking, service life estimations

1 Introduction

Hydro turbine components are exposed to high mechanical loadings and corrosion. Fatigue, erosion and cavitation are the main factors which may lead to failure and therefore to expensive maintenance activities.

The analysis regarding the working conditions showed that the cracking occurred, Fig. 1, in one of the turbines from hydropower plants cascade, which operated at a higher head than the rest.

Fig.1 The cracked runner blade

The technical characteristics of the damaged turbine are:

- ✓ runner diameter - 5500 mm
- ✓ nominal speed - 115.4 rpm
- ✓ maximum power for net head - 35.5 MW
- ✓ maximum head - 28.20 m
- ✓ net head - 24.0 m
- ✓ minimum head - 16.0 m

Fig.2 shows the path of the investigated crack, which penetrated the blade and developed to a final length of 600 mm, measured on the pressure side.

Fig.2 The crack on the pressure side

In order to define the causes that led to the failure of the blade, the authors carried out both metallographic investigations and numerical analysis regarding the resistance of the blade and service life estimations.

2 Metallographic Investigations

The sample for metallographic investigations was cut from the cracked blade as indicated in Fig.3.

Fig.3 Position of the metallographic sample

The macroscopic examination of the fracture surface (Fig. 4), revealed the specific appearance of fatigue cracking [1]. The surface is smoothened, resulting from the relative friction of the two pieces of the cracked blade one upon the other, during the alternative loads. The positions of the fan-shaped striations indicate that the cracking started from the region marked with "SP" (starting point) in Fig.4 The SEM-micrographs of the regions marked with "a" and "b" are presented in Fig.5.

Fig.4 Macrograph of the fracture surface

The images shown in Fig.5 indicate a high content of non-metallic inclusions in the blade material (marked with 1 in Fig.5.a). During the crack propagation, the operating water determined the corrosion of the base material surrounding these inclusions. As a consequence, the non-metallic inclusions released from the surface, leaving craters behind (position 2 in Fig.5.b), which were filled in with corrosion products (position 3 in Fig. 5.b).

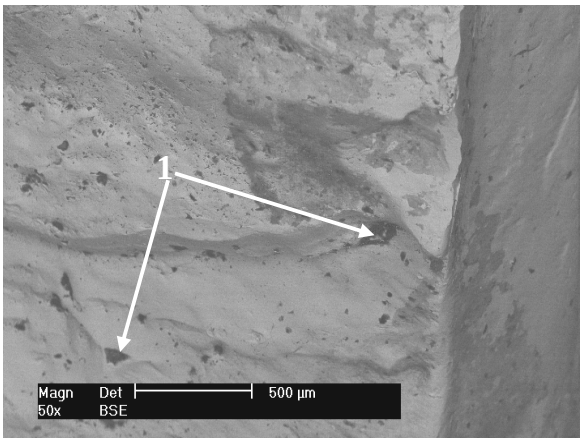

a – BSE-image, 50x

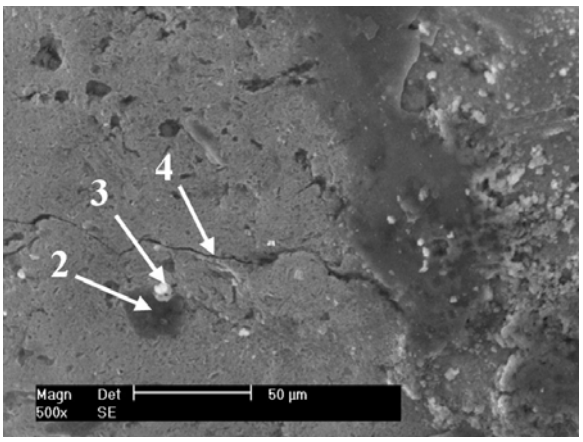

b – SE-image, 500x

Fig.5 SEM-micrographs of the fracture surface

In the surface of the investigated sample numerous secondary cracks (as marked by 4 in Fig.5.b) were observed, which are specific for fatigue cracking [2], [3].

After SEM-examination, the crack surface was grinded, polished and examined with the scanning electron microscope (Philips XL30 ESEM). Globular non-metallic inclusions could be observed, as well as the surrounding corrosion attack of the metallic material, Fig.6.a. The XRD-analyze led to the conclusion, that these inclusions are silicates and oxides, Fig.6.b.

In order to visualize the structure of the blade material, the sample was etched using a V2A-solution and was examined with the light microscope (LEICA DM 6000M). As shown in Fig.7, the microstructure is consisting of martensite, containing a high percentage of ferrite, with grid-like distribution. The presence of numerous non-metallic inclusions is attested also by these images.

The metallographic investigations led to the conclusion that the cracking of the blade was caused by fatigue and was initiated by non metallic inclusions existing in the vicinity of the blade surface. The crack propagation occurred gradually, through development of the principal fracture front. Because of the high content of non-metallic inclusions and the inhomogeneous structure of the blade material, additionally numerous secondary cracks developed inside the material.

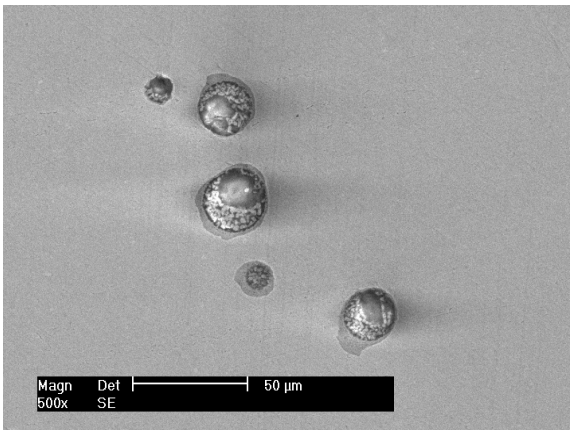

a - SEM-micrograph

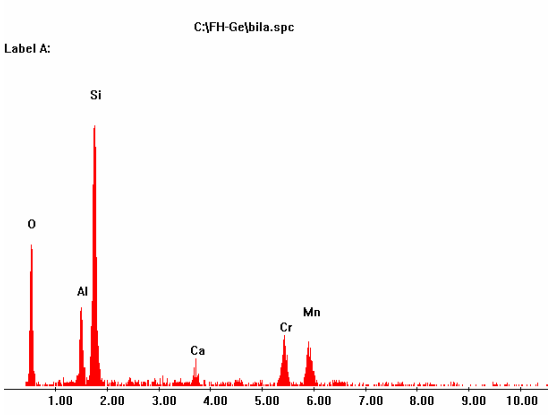

b - XRD-capture of the inclusions

Fig.6 Non-metallic inclusions in the vicinity of the crack surface

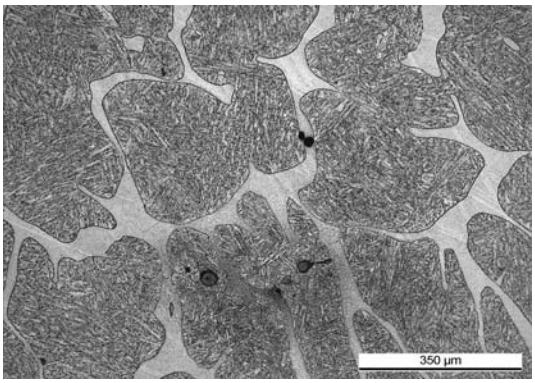

a – 200x

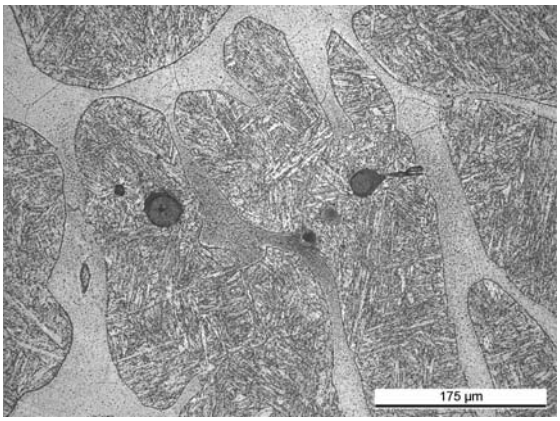

b – 500x

Fig.7 Structure of the blade material

After the failure was initiated, the fracture surfaces were exposed to chemical corrosion. This phenomenon was accentuated and accelerated by the presence of the high content of non metallic inclusions.

3 Numerical Investigations

Numerical investigations regarding the resistance and service life estimations of the blade included the following steps:

- the 3D solid modeling of the runner blade, using the Autodesk Inventor software;
- determination of the blade loads starting from hydrodynamic conditions;
- linear static analyses, for different stress relieve groove geometries and blade numbers;
- service life estimations, calculated for maximal stress values of the concentrators resulted from the COSMOS Design Star software, using the Haigh fatigue diagram.

3.1 3D solid modeling of the runner blade

The axial blade turbine has a very complex geometry, which must be generated in a Computer Aided Software (CAD) for the final blade drawing and for finite elements resistance calculations. Autodesk Inventor was chosen as CAD software. The purpose of the modeling process is to obtain the blade as a solid object and not as a surface, so that it may be used for finite elements resistance calculations. Therefore the following steps are required:

- starting with the plane coordinates of the profiles, the 3D coordinates disposed on cylinders to the radius specified in execution drawings of the runner were calculated, Fig.8;

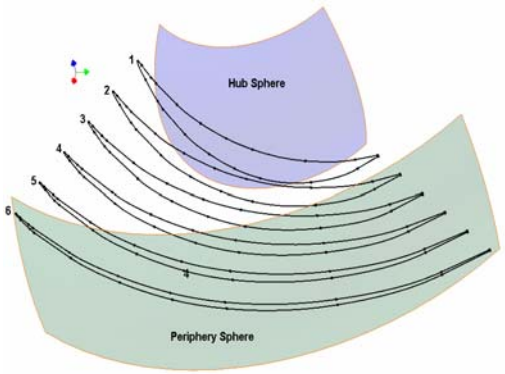

Fig.8 Blade profiles disposed on cylinders

- generation of the suction side surface, pressure side surface and leading edge surface, based on closed loops of the 3D coordinates disposed on cylinders, Fig.9;

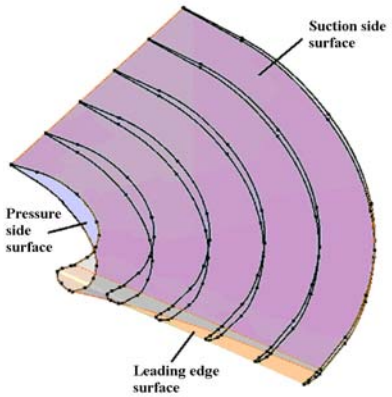

Fig.9 Suction side surface, pressure side surface and leading edge surface of the blade

- extensions of blade's surfaces: the previous surfaces must be extended to the hub and periphery direction to obtain the surfaces of the complete blade, Fig.10;

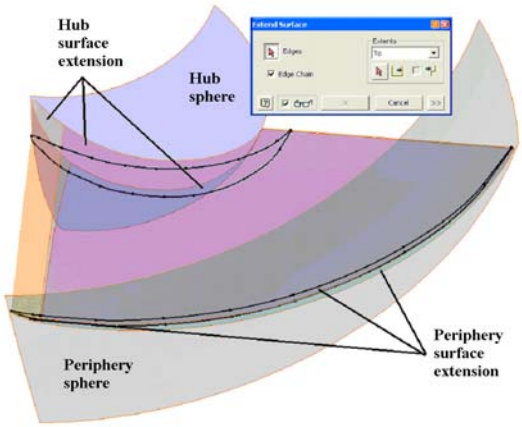

Fig.10 Extensions of blade's surfaces

- intersections of the blade surfaces with radial planes, disposed at imposed angles, Fig.11, which will generate a number of closed loops disposed on radial planes, Fig.12;

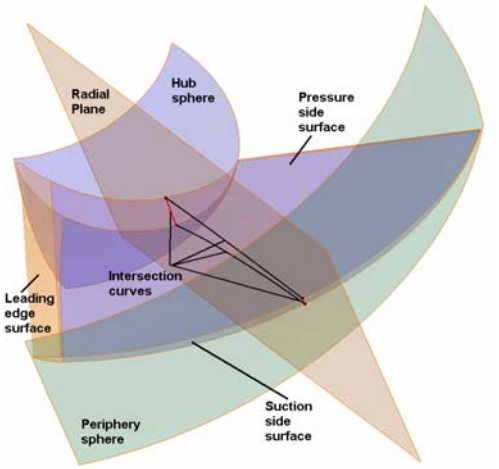

Fig.11 Intersection curves for a radial plane

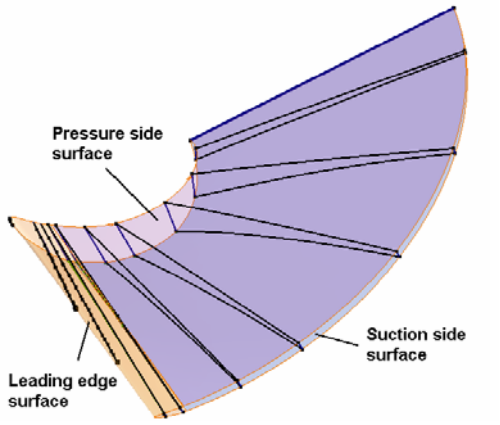

Fig.12 Intersection curves for multiple radial planes

- generation of the solid model of the blade, based on the previous closed loops, Fig.13;

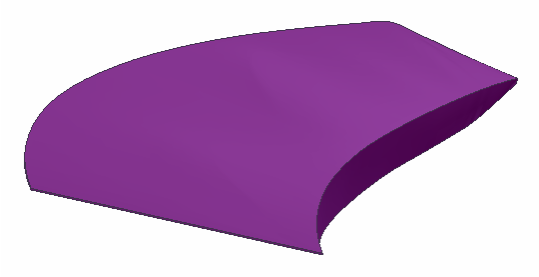

Fig.13 Solid model of the blade

- completion of the 3D solid geometry of the blade with the flange and stress relieve groove with different geometry, Fig.14 and Fig.15.

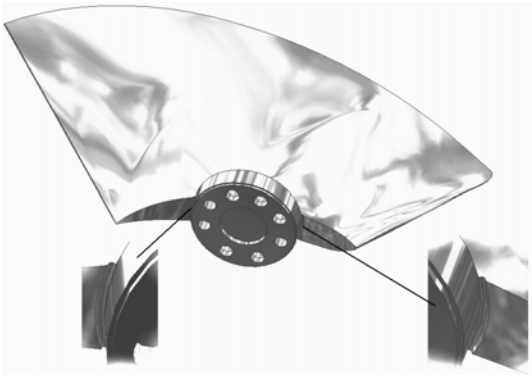

Fig.14 The solid model of the blade with stress relieve groove R8x20

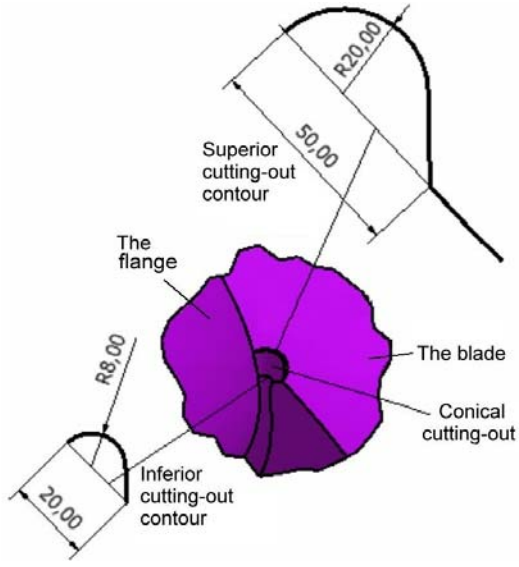

Fig.15 The geometry of the stress relieve groove R20x50

3.2 Determination of the blade loads from hydrodynamic conditions

The hydrodynamic loads applied on the axial runner are presented in Fig.16:

- the gravity load $\vec{G}$; from Inventor software results the blade mass ~ 4000 kg;
- the centrifugal force $\vec{F_C}$ generated for the runner speed 115.4 rot/min;
- the axial thrust $\vec{F_{AH}}$, resulted from the measurements on model;
- the tangential force $\vec{F_T}$, which contribute to the machine couple;
- $\vec{R}$ is the resultant of the hydraulic force on the blade;
- "e" is the distance between blade axis and the resultant direction $\vec{R}$.

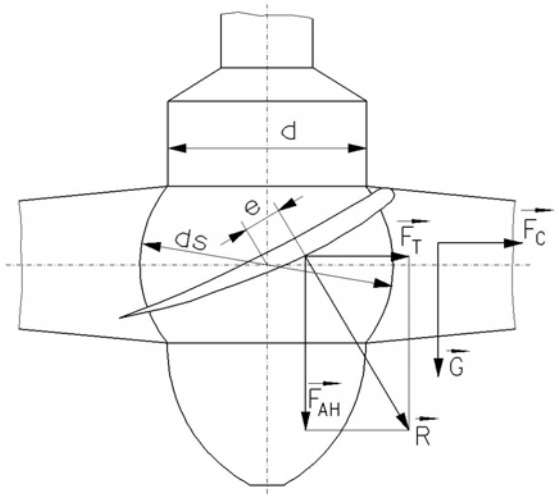

Fig.16 The hydrodynamic loads applied to the runner

The operation points considered for resistance calculus correspond to the following power values: 35.5 MW, 30 MW, 25 MW, 20 MW and 15 MW at different head values.

The axial thrust and tangential forces were calculated for 4 and 6 runner blades, Table 1 and Table 2.

Table 1 Operating points for resistance calculus – the real case of 4 blades

Point	Power	Head	Flow	Axial thrust	Tangential force
	P	H	Q	F_{AH}/blade	F_T/blade
	MW	m	m^3/s	KN	KN
1.	35.5	28.2	143.59	878.6	381.5
2.	35.5	24	168	762.3	381.5
3.	30	28.2	121.9	878.6	322.4
4.	30	24	140.62	771.4	322.4
5.	30	23	146.25	747.9	322.4
6.	30	22	153.12	715.4	322.4
7.	25	28.2	102.56	863.7	268.7
8.	25	24	118.03	780.5	268.7
9.	25	23	122.48	761.8	268.7
10.	25	22	127.24	732.1	268.7
11.	25	21	132.98	698.8	268.7
12.	20	27.5	84.74	873.5	214.9
13.	20	24	95.65	795.0	214.9
14.	20	23	99.43	765.3	214.9
15.	20	22	103.4	740.4	214.9
16.	20	21	176.81	675.0	214.9
17.	15	23	75.84	765.3	161.2
18.	15	22	79.08	743.7	161.2
19.	15	21	82.54	722.6	161.2

Table 2 Operating points for resistance calculus – the hypothetically case of 6 blades

Point	Power	Head	Flow	Axial thrust	Tangential force
	P	H	Q	F_{AH}/blade	F_T/blade
	MW	m	m^3/s	KN	KN
1.	35.5	28.2	143.59	585.8	254.3
2.	35.5	24	168	508.2	254.3
3.	30	28.2	121.9	585.8	214.9
4.	30	24	140.62	514.3	214.9
5.	30	23	146.25	498.6	214.9
6.	30	22	153.12	476.9	214.9
7.	25	28.2	102.56	575.8	179.1
8.	25	24	118.03	520.3	179.1
9.	25	23	122.48	507.9	179.1
10.	25	22	127.24	488.0	179.1
11.	25	21	132.98	465.9	179.1
12.	20	27.5	84.74	582.3	143.3
13.	20	24	95.65	530.0	143.3
14.	20	23	99.43	510.2	143.3
15.	20	22	103.4	493.6	143.3
16.	20	21	176.81	450.0	143.3
17.	15	23	75.84	510.2	107.5
18.	15	22	79.08	495.8	107.5
19.	15	21	82.54	481.7	107.5

The placement of the operating points cover the area of the turbine operation and are shown in the prototype hill chart H-Q from Fig.17.

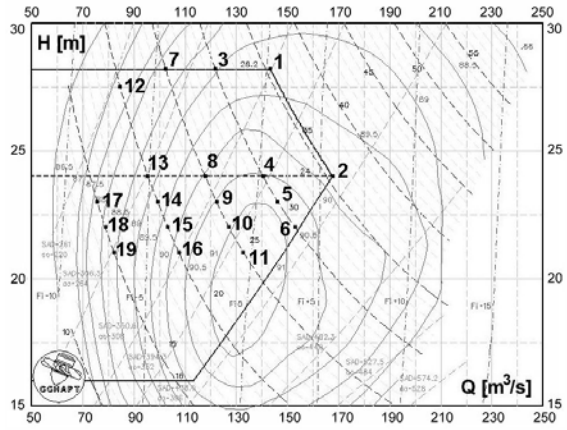

Fig.17 The placement of the operating points in the prototype hill chart

3.3 Linear static analyses, for different stress relieve groove geometries and blade numbers

The numerical study was made with the Cosmos Design Star software, which offers a wide range of advanced type analyses: linear static analysis and nonlinear analysis, frequency analysis, linearized buckling analysis and thermal analysis.

Fig.18 shows the loads and restrictions applied to the blade:

- fixed type constraints applied to the flange holes, which impose 0 value for the translations and rotations of the selected entities;
- axial thrust F_{AH};
- tangential force F_T;
- centrifugal force F_C;
- blade gravity G.

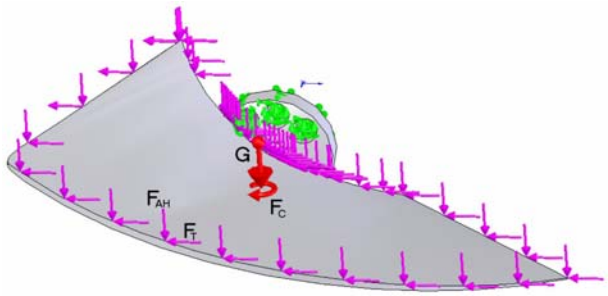

Fig.18 Loads and restrictions applied to the blade in the finite element software

Because the blade cannot be generated as a surface with constant thickness, for finite element analyze, only solid mesh (parabolic tetrahedral solid elements) can be used.

In meshing a part or an assembly with solid elements, the software generates one of the following types of elements based on the active mesh options:

- draft quality mesh; the automatic mesher generates linear tetrahedral solid elements; linear elements are also called first-order;
- high quality mesh; the automatic mesher generates parabolic tetrahedral solid elements; parabolic elements are also called second-order.

In general, for the same mesh density (number of elements), parabolic elements yield better results than linear elements because: they represent curved boundaries more accurately and they produce better mathematical approximations. However, parabolic elements require greater computational resources than linear elements. For structural problems, each node in a solid element has three degrees of freedom that represent the translations in three orthogonal directions.

The mesh is shown in Fig. 19. For original stress relieve groove R8x20 a local fine mesh was used, Fig. 12. The results are presented numerically in Table 3, and graphically in Fig. 21 and Fig. 22, only for operating point no. 1.

Fig.19 The blade mesh

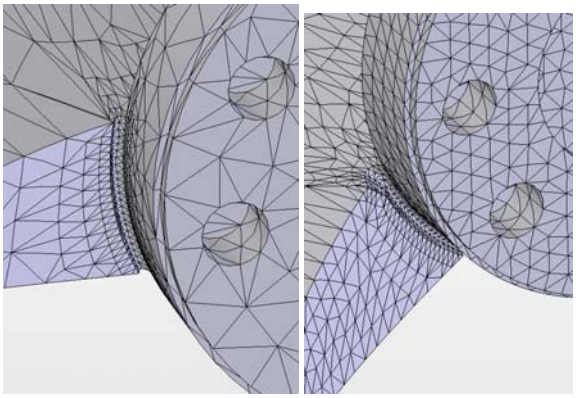

Fig.20 The blade mesh in the stress relieve groove area

Table 3 Numerical results for stress relieve groove R8x20 (4 blades)

Operation point	Head H [m]	Power P [MW]	Von Mises Stress	Max. Displacement
1	28.2	35.5	474.7	20.47
2	24	35.5	434.0	17.97
3	28.2	30	467.7	20.27
4	24	30	447.5	17.55
7	28.2	25	475.4	19.32
8	24	25	444.6	17.57
12	27.5	20	472.7	19.35
13	24	20	443.6	17.7
17	23	15	426.4	16.91

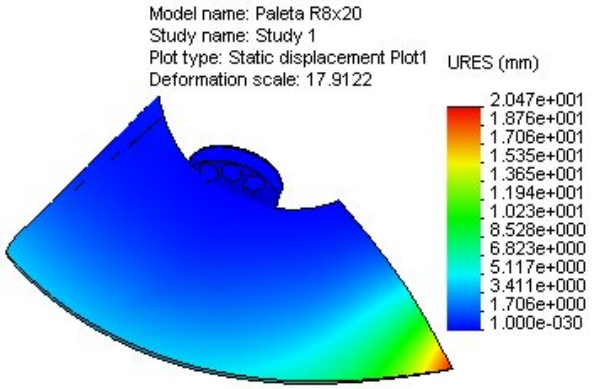

Fig.21 The resultant displacement plot - Point 1 stress relieve groove R8x50 (4 blades)

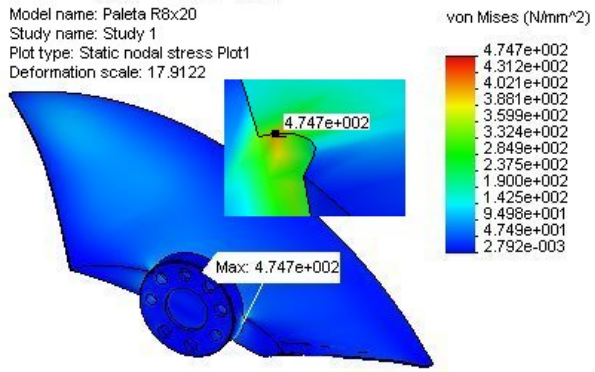

Fig.22 The Von Mises stress plot - Point 1 stress relieve groove R8x50 (4 blades)

To reduce the maximal stress values, the geometry of the stress relieve groove was modified from R8x20 to R20x50, Fig.15. The results are numerically shown in Table 4.

Table 4 presents a reducing of the Von Mises stress values for a power range of 30…15 MW, but not enough to promote the solution. In these circumstances, the blade loads can be reduced by blade number increasing.

Table 5 shows the numerical results for stress relieve groove R8x20 with 6 blades. A significant decreasing of the stress and displacements values can be observed, comparing with the previous solutions.

Table 4 Numerical results for stress relieve groove R20x50 (4 blades)

Operation point	Head H [m]	Power P [MW]	Von Mises Stress	Max. Displacement
1	28.2	35.5	426.3	20.47
2	24	35.5	388.8	17.97
3	28.2	30	421.0	20.28
4	24	30	386.4	17.98
7	28.2	25	411.4	19.78
8	24	25	384.6	17.99
12	27.5	20	409.8	19.82
13	24	20	384.5	18.13
17	23	15	370.1	17.32

Table 5 Numerical results for stress relieve groove R20x50 (6 blades)

Operation point	Head H [m]	Power P [MW]	Von Mises Stress	Max. Displacement
1	28.2	35.5	357.3	13.76
2	24	35.5	330.0	12.09
3	28.2	30	352.7	13.63
4	24	30	339.9	11.82
7	28.2	25	358.4	12.99
8	24	25	337.9	11.83
12	27.5	20	356.6	13.01
13	24	20	337.3	11.92
17	23	15	325.8	11.39

The Von Mises values are presented graphically in the Fig. 23, Fig. 24, Fig. 25 and Fig 26 for the power steps P=35.5 MW, P=30 MW, P=25 MW and P=20 MW. The displacement values are presented graphically in the Fig. 27.

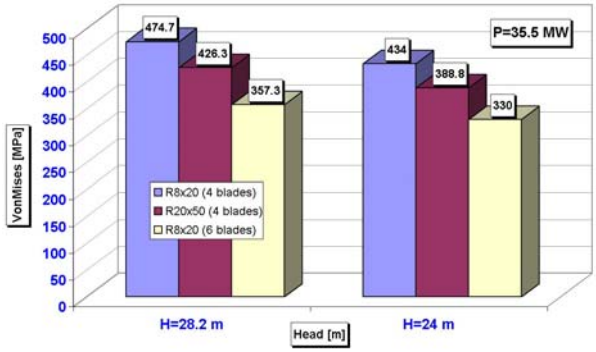

Fig.23 The comparison between Von Mises values for power step P=35.5 MW

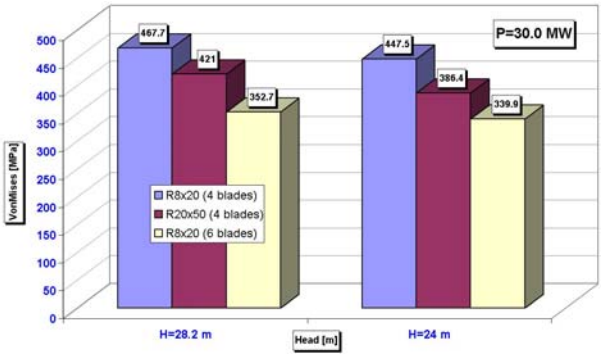

Fig.24 The comparison between Von Mises values for power step P=30.0 MW

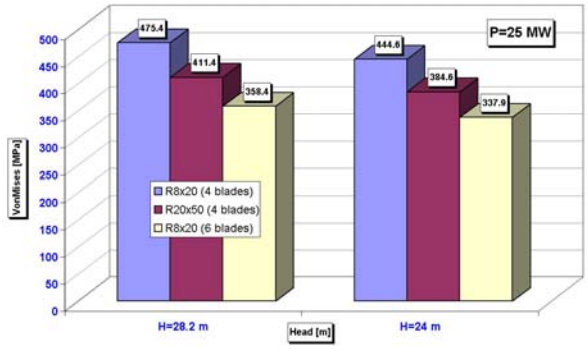

Fig.25 The comparison between Von Mises values for power step P=25.0 MW

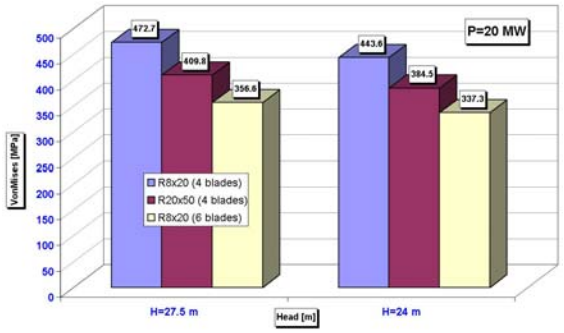

Fig.26 The comparison between Von Mises values for power step P=20.0 MW

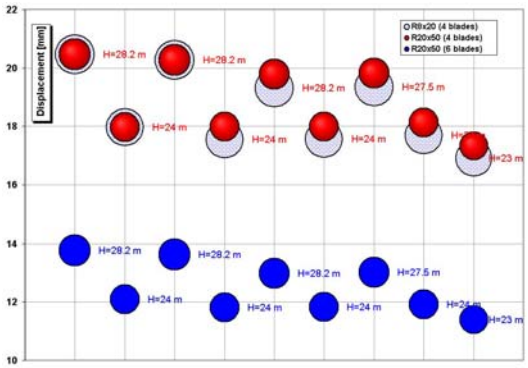

Fig.27 The comparison between displacement values for all power steps

From all previous figures, the decreasing of the VonMises values from the initial geometry solution of the stress relieve groove R8x20 (4 blades), to the solutions R20x50 (4 blades) and R20x50 (6 blades) is obvious. The same conclusion is obtained for displacement, from the geometry solution of the stress relieve groove R8x20 (4 blades) or R20x50 (4 blades) to R20x50 (6 blades) solution.

3.4 Service life estimations

For service life estimations a standard procedure for hydraulic turbine is used, for the operating points with maximal stress values. The amplitude oscillation for Kaplan blade turbine is experimentally obtained and is around 20 MPa.

The yield strength value of the blade material is $R_{P0,2\ min}$=550 MPa. The calculated values of the stress for stress relieve groove R8x20 and R20x50 and 4 blades were introduced in Haigh diagram, Fig. 28 [4].

From the Haigh diagram results that, for stress relieve groove R8x20, the blade cracks should be obtained between $10^9 \div 10^{10}$ of the fatigue cycles. To reduce the stress concentrator values, a number of different stress relieve groove geometry were studied. The optimal solution was obtained for stress relieve groove R20x50, where the stress values were reduced in the range between 45...60 MPa (see Table 4 and Fig. 28), but not enough to promote as a final solution.

The results from Fig.27 are ideally, because the fatigue curves are obtained in laboratory for samples with controlled chemical composition and homogeneity, with no fissures and surfaces or deeply defects. For these reasons, in service life estimations and fatigue calculus is recommended that the stress concentrator values will not be higher than half of yield strength value of the material, in our case 275 MPa.

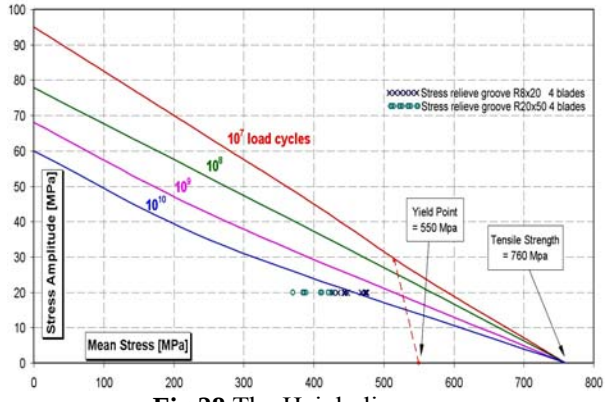

Fig.28 The Haigh diagram

4 Conclusions

The metallographic investigations and the calculations carried out led to the conclusion that the cracking of the blade started and developed from the stress concentrator placed between blade and blade flange on the leading edge direction.

A few stress relieve groove geometry were analyzed, but did not generate a decreasing of the stress concentrators in admissible limits (smaller than half of yield strength value of the material). This effect cannot be obtained only by modifying the stress relieve groove geometry.

In order to decrease the maximal stress value it is necessary to reduce the hydrodynamic loads on the blade. For existing operating conditions (discharge, head, speed, power), the stress decreasing is possible only by increasing the number of the runner blades.

In order to verify this conclusion, for the same blade geometry, a blade with stress relieve groove R8x20 was calculated, but for 6 blades. The results show a significant decreasing of the stress concentrators values (about 100 MPa) which, associated with an optimal stress relieve groove geometry, can lead to a stress reducing in admissible limits. These calculations are theoretically, because they are made for a runner with 6 blades and the same geometry of the blade. But, a new runner, with 5 or 6 blades, will require a new blade geometry (new profiles, a blade with a smaller extensions), and, therefore, the loads will be modified [5], [6], [7], [8].

Acknowledgement

The work has been supported by the MATNANTECH program, project CEEX-M1-C2-1185, Contract no. 64, acronym iSMART-flow. Numerical computations and experimental investigations have been performed at the ExpertLAB from the Research Centre for Hydraulics, Automation and Thermal Processes, „Eftimie Murgu" University of Reşiţa, www.cchapt.ro.

References:

[1] Lange G., *Systematische Beurteilung technischer Schadensfälle*, *5.Auflage,* Wiley - VCH Verlag, D-69469 Weinheim, Germany, 2001, pp. 103-147.

[2] Lange G., *Systematische Beurteilung technischer Schadensfälle*, *5.Auflage,* Wiley - VCH Verlag, D-69469 Weinheim, Germany, 2001, pp. 163.

[3] Schmidt P.F., *Praxis der Rasterelektronen-mikroskopie und Mikrobereichsanalyse*, Expert Verlag, Renningen - Malmsheim, Germany, 1994, pp. 103-147.

[4] Helmuth K., *Stakeholders perspectives on the challenges or threats and on "A European research network as one instrument to effective rehabilitation and utilization of European hydropower Infrastructure"*, Elforsk Workshop, Stockholm, Sweden, June 29th 2004.

[5] A. Iosif, I. Sarbu, *Simulation of velocities and pressures distribution on blade of pump-turbine runner*, Proceedings of the 5th IASME / WSEAS International Conference on CONTINUUM MECHANICS (CM '10), University of Cambridge, UK, February 23-25, 2010, pp 190-195.

[6] A. Rosca, D. Rosca, V. Nastasescu, *Consideration on Stainless Steel Plate Plastic Deformed by Fluid Impact Substances and Pressured Nitrogen Blasting*, WSEAS TRANSACTIONS on APPLIED and THEORETICAL MECHANICS, Volume 3, 2008, ISSN: 1991-8747.

[7] G. Pengcheng, L. Xingqi, L. Weili, Z. Xiaobo, L. Peng, *Effect of blade geometric parameters on the operating stability of the hydraulic turbine*, Proceedings of the 4th WSEAS International Conference on Fluid Mechanics and Aerodynamics, Elounda, Greece, August 21-23, 2006, pp 315-318.

[8] Sukhvinder K. B., Shyamala K., V. Chaitanya, Kedarinath, I.N. Niranjan Kumar, *Steady state stress analysis and heat transfer* analysis *on an axial flow gas turbine blades and disk*, Proceedings of the 2006 IASME/WSEAS International Conference on Energy & Environmental Systems, Chalkida, Greece, May 8-10, 2006, pp110-116.